11th World Congress on Computational Mechanics (WCCM XI)
5th European Conference on Computational Mechanics (ECCM V)
6th European Conference on Computational Fluid Dynamics (ECFD VI)
E. Oñate, J. Oliver and A. Huerta (Eds)

PRELIMINARY DEVELOPMENTS TOWARDS A HIGH-ORDER AND EFFICIENT LES CODE FOR PROPULSION APPLICATIONS

FRANCESCO CAPUANO*, ANDREA MASTELLONE*, SARA DI BENEDETTO*, LUIGI CUTRONE* AND ANTONIO SCHETTINO*

* Centro Italiano Ricerche Aerospaziali (CIRA)
Propulsion Unit
via Maiorise snc, 81043 Capua (CE), Italy
e-mail: f.capuano@cira.it, web page: http://www.cira.it/

Key words: Compact schemes, large-eddy simulation, combustion

Abstract. An advanced LES code, named *SPARK-LES*, is currently under development at CIRA within the frame of the HYPROB program. SPARK-LES is a structured, multi-block finite-volume code that solves the compressible Navier-Stokes equations with the final goal of performing accurate simulations of high-pressure combustion with suitable numerical/physical models. In this paper, the key features of the computational core are described. Centered high-order explicit and compact schemes for space integration are implemented; different solutions to improve numerical stability and robustness are analyzed and discussed. The capabilities of the code to reproduce the essential features of turbulent dynamics are proved by simulating the well-known Taylor-Green vortex problem.

1 INTRODUCTION

Large-Eddy (LES) and Direct Numerical Simulation (DNS) are nowadays regarded as powerful and reliable techniques in the framework of combustion and propulsion applications [1]. While for DNS the current computing power available is still far from enabling a time-accurate and fully-resolved solution of the entire mathematical model, LES is believed to be a good compromise between computational cost and accuracy. Its usage in turbulent reacting flows has grown significantly over the last decade, especially for low-pressure flames [2]; however, a number of recent encouraging results advocate the application of LES to high-pressure combustion as well [3]. The inherent ability of LES to capture the essential dynamics of unsteady phenomena on a wide range of space- and time-scales makes it a valuable tool for both design and research purposes.

In this perspective, the LES code *SPARK-LES* is currently being developed at CIRA in the frame of the HYPROB Program [4], funded by the Italian Ministry of Research.

The Program's main objective is to improve national system and technology capabilities in hybrid- and liquid-rocket engines for future space applications; for the latter, the main interest is on LOX/LCH4 technology. The development of a LES code is one of the on-going research lines of the Program. In a timeframe of four years, the code shall be able to 1) provide an advanced analysis tool for design purposes, and 2) reproduce the main physical phenomena occurring within a liquid-rocket thrust chamber (e.g., turbulent mixing, high-pressure combustion, acoustic instabilities) with high-fidelity numerical methods and state-of-the-art modelling.

The paper is focused on the initial part of the development activity, namely the design and implementation of the code computational core. The aforementioned phenomena occur on a wide range of turbulent scales and therefore high-order schemes with good resolution properties are needed. Classical centered schemes are not dissipative in nature, but suffer from significant dispersion errors due to their limited stencil [5]. In contrast, compact schemes are able to provide better resolution on equal order of accuracy by mimicking a spectral behaviour [6]. Compact schemes are widely used in a finite-difference context, but are much more rarely applied in a finite-volume framework [7, 8]. The latter combination appears to be advantageous, by combining the accuracy of compact schemes with the conservation property of finite-volume methods.

The demand for stability and robustness is also taken into consideration. Usual methods include artificial dissipation or filtering of the flowfield, while more refined approaches aim to enforce secondary conservation properties, such as kinetic energy preservation. It has been proved that the overall stability and accuracy of the scheme notably improves if quadratic invariants are preserved at a discrete level [9].

The scope of the present work is to prove that the baseline numerical method is able to accurately reproduce the essential features of turbulent dynamics with high computational efficiency. To this aim, two classical benchmarks have been considered, the convection of a subsonic vortex [10] and the well-known Taylor-Green vortex problem [11]. The former is an excellent verification of the dissipation and dispersion properties of the scheme, while the latter allows to validate the numerical algorithm on a protoype turbulent flow. Simulations are performed by directly solving the Navier-Stokes equations without use of any subgrid-model in order to isolate numerical errors also in under-resolved cases.

The paper is organized as follows. In Section 2, the governing equations are briefly recalled. Then, the numerical method is introduced in Section 3. Results are finally presented in Section 4.

2 GOVERNING EQUATIONS

In this work, the compressible, non-reacting Navier-Stokes equations in conservative form are considered. In a three-dimensional Cartesian coordinate frame (x, y, z), the motion of a gas with density ρ, velocity $\mathbf{u} = (u, v, w)$, pressure p, temperature T and

total energy E is governed by the system:

$$\frac{\partial \mathbf{U}}{\partial t} + \frac{\partial \mathbf{F}_x}{\partial x} + \frac{\partial \mathbf{F}_y}{\partial y} + \frac{\partial \mathbf{F}_z}{\partial z} = 0, \tag{1}$$

where $\mathbf{U}$ is the vector of conservative variables, $\mathbf{U} = (\rho, \rho u, \rho v, \rho w, E)$. The vectors $\mathbf{F}_x = \mathbf{F}_x^c - \mathbf{F}_x^d$, $\mathbf{F}_y = \mathbf{F}_y^c - \mathbf{F}_y^d$ and $\mathbf{F}_z = \mathbf{F}_z^c - \mathbf{F}_z^d$ represent the fluxes along the three components. The inviscid (convective) fluxes are defined as:

$$\mathbf{F}_x^c = \begin{pmatrix} \rho u \\ \rho u^2 + p \\ \rho uv \\ \rho uw \\ u(E+p) \end{pmatrix}, \quad \mathbf{F}_y^c = \begin{pmatrix} \rho v \\ \rho uv \\ \rho v^2 + p \\ \rho vw \\ v(E+p) \end{pmatrix}, \quad \mathbf{F}_z^c = \begin{pmatrix} \rho w \\ \rho uw \\ \rho vw \\ \rho w^2 + p \\ w(E+p) \end{pmatrix}, \tag{2}$$

whereas the diffusive fluxes are

$$\mathbf{F}_x^d = \begin{pmatrix} 0 \\ \tau_{11} \\ \tau_{12} \\ \tau_{13} \\ (\tau \mathbf{u})_1 - q_1 \end{pmatrix}, \quad \mathbf{F}_y^d = \begin{pmatrix} 0 \\ \tau_{21} \\ \tau_{22} \\ \tau_{23} \\ (\tau \mathbf{u})_2 - q_2 \end{pmatrix}, \quad \mathbf{F}_z^d = \begin{pmatrix} 0 \\ \tau_{31} \\ \tau_{32} \\ \tau_{33} \\ (\tau \mathbf{u})_3 - q_3 \end{pmatrix}. \tag{3}$$

The stress tensor τ_{ij} and the conductive heat flux q_i are expressed by the usual Newton's and Fourier's laws, respectively $\tau_{ij} = \mu \left(\frac{\partial u_i}{\partial x_j} + \frac{\partial u_j}{\partial x_i} - \frac{2}{3}\delta_{ij} \frac{\partial u_k}{\partial x_k} \right)$ and $q_i = -\lambda \frac{\partial T}{\partial x_i}$, where μ is the molecular viscosity and λ the thermal conductivity of the fluid. The code is provided with a full real-gas thermodynamic package; here, closure is achieved by means of the ideal-gas equation of state, $p = \rho RT$.

3 NUMERICAL METHOD

Most of the success of turbulent simulations relies on the use and construction of accurate discretization methods, in order to compute unsteady turbulent structures on a wide range of space- and time-scales without significant numerical contamination. It is widely recognized that ideal numerical schemes for LES and DNS should have the following properties:

- discrete conservation of primary unknowns;
- high-order accuracy and good spectral properties in smooth regions of the flow;
- stability and robustness.

The fulfilment of these confilicting requirements is not a trivial task. While discrete conservation of linear invariants can be obtained by casting the discrete equations in

a locally conservative form, high-order accuracy often comes into opposition with the robustness of the scheme. These aspects have been taken into consideration carefully in the design and development of the computational core of the code, and will be discussed and motivated throughout the following sections.

3.1 Finite-volume discretization

The computational domain is partitioned into a structured grid of hexahedrons indexed by (i, j, k). The finite-volume method is based upon integration of Eq. (1) over a generic control volume Ω, yielding

$$V_{ijk}\frac{\partial \bar{\mathbf{U}}_{ijk}}{\partial t} + \int_{\partial\Omega} (\mathbf{F}_x n_x + \mathbf{F}_y n_y + \mathbf{F}_z n_z)\, d\sigma = 0, \tag{4}$$

where $V_{ijk} = |\Omega|$ and

$$\bar{\mathbf{U}}_{ijk} = \frac{1}{V_{ijk}} \int_{\Omega} \mathbf{U} d\Omega. \tag{5}$$

The integral Eq. (4) applies to each control-volume; as a consequence, surface integrals over inner cell faces cancel out and discrete global conservation of primary unknowns is guaranteed through the *telescopic* property. The built-in global conservation feature is one of the major advantages of finite-volume methods and formally accomplishes the first of the requirements listed in §3.

The meaning of the cell integral in Eq. (5) requires further discussion. In a so-called *pointwise* approach, nodal values $\mathbf{U}_P$ are usually supposed to be known at the cell-center, resulting in a second-order accurate average, i.e., $\bar{\mathbf{U}} = \mathbf{U}_P + \mathcal{O}(V^2)$. Therefore, if high-order accuracy is seeked, correspondent high-order formulas are needed for the evaluation of the integral. However, a more careful look at Eq. (4) suggests to store and advance in time the cell average values themselves. In this approach, known as *cell-averaged*, the integral has not to be evaluated and the accuracy of the method depends solely on the fluxes reconstruction [7]. The cell-averaged approach is adopted here and will be used throughout the paper.

The solution algorithm follows that of any typycal semi-discrete method, in which Eq. (4) is first semi-discretized in space and then advanced in time.

3.2 Spatial discretization

The surface fluxes appearing in Eq. (4) need to be properly approximated. Without loss of generality, the cell interface $S_{i-1/2}$ along a generic (j, k) line and between cells (i) and $(i-1)$ will be considered hereinafter. The corresponding flux is defined by:

$$\tilde{\mathbf{F}}_{i-1/2} = \int_{S_{i-1/2}} (\mathbf{F}_x n_x + \mathbf{F}_y n_y + \mathbf{F}_z n_z)\, d\sigma \approx S\left(\tilde{\mathbf{F}}_x n_x + \tilde{\mathbf{F}}_y n_y + \tilde{\mathbf{F}}_z n_z\right), \tag{6}$$

where $S = \left|S_{i-1/2}\right|$. It is assumed that the normal vector is constant along the interface, while the operator $\tilde{(\cdot)}$ denotes surface averaging. Starting from Eq. (6), the discretizations of convective and diffusive fluxes will be described separately in the next sections.

3.2.1 Convective fluxes

The convective fluxes are evaluated using face-averaged values of conservative variables:

$$\tilde{\mathbf{F}}^c_{i-1/2} = S\left(\mathbf{F}^c_x(\tilde{\mathbf{U}}_{i-1/2})n_x + \mathbf{F}^c_y(\tilde{\mathbf{U}}_{i-1/2})n_y + \mathbf{F}^c_z(\tilde{\mathbf{U}}_{i-1/2})n_z\right). \tag{7}$$

The core of the method, as well as most of the code overall accuracy, lies on a proper interpolation of conservative variables to cell faces. Indeed, it is well-known that discretization of non-linear convective fluxes is crucial for a correct representation of the turbulent energy cascade, by ensuring that 1) the energy-carrying scales are resolved appropriately, and 2) numerical dissipation does not interfere with the energy transfer process (in DNS) or with the subgrid-scale model (in LES). Low dissipation schemes with good spectral properties are mandatory for an accurate simulation of turbulent dynamics. In light of this, non-dissipative centered explicit and compact schemes have been implemented [6].

Following [8], face-averaged values are obtained by means of a *cartesian-like* approach, i.e., $\mathbf{U}$ is assumed to depend exclusively on the curvilinear abscissa along each line of the grid. Under this hypothesis, the face-averaged value $\tilde{\mathbf{U}}$ at the interface $(i-1/2, j, k)$ is expressed by the following interpolation formula:

$$\alpha\tilde{\mathbf{U}}_{i-3/2} + \tilde{\mathbf{U}}_{i-1/2} + \alpha\tilde{\mathbf{U}}_{i+1/2} = \sum_{l=1}^{L} \gamma_l \left(\bar{\mathbf{U}}_{i-l} + \bar{\mathbf{U}}_{i+l-1}\right). \tag{8}$$

Eq. (8) represents a generic family of explicit ($\alpha = 0$) or implicit ($\alpha \neq 0$) centered interpolation formulas based on cell-averaged values. The coefficients α, L and γ_l determine the order of accuracy and the spectral properties of the scheme. In Table 1, a number of possibilities are given, assuming uniform grid-spacing Δ, along with the corresponding acronym used in the work. A second-order explicit (2E) and fourth-order explicit (4E) and compact (4C) schemes are considered in this work. For non-uniform grids, the coefficients involve the metrics of the mesh and are calculated by matching the Taylor series coefficients expansion of various orders.

It is useful to recall that the formal truncation error of a scheme is an integral measure of the local error over all wavenumbers in the asymptotic limit of grid-refinement. Thus, it does not provide any information on how the approximation behaves over the entire range of length scales a given mesh can resolve. An appropriate tool to quantify the *resolution* characteristics is the Fourier analysis [6]. The discrete operator is applied to a single Fourier wave e^{ikx} advecting linearly with speed c, where k is the wavenumber. The discrete approximation produces a *modified wavenumber*, k', whose imaginary part

Table 1: Interpolation schemes considered in the work.

Scheme	α	L	γ_1	γ_2	Order
2E	0	1	1/2	0	$\mathcal{O}(\Delta^2)$
4E	0	2	7/12	−1/12	$\mathcal{O}(\Delta^4)$
4C	1/4	1	3/4	0	$\mathcal{O}(\Delta^4)$

Figure 1: Spectral properties of interpolation schemes. *Left.* Modified wavenumber as a function of the wavenumber. *Right.* Modified phase speed as a function of the wavenumber.

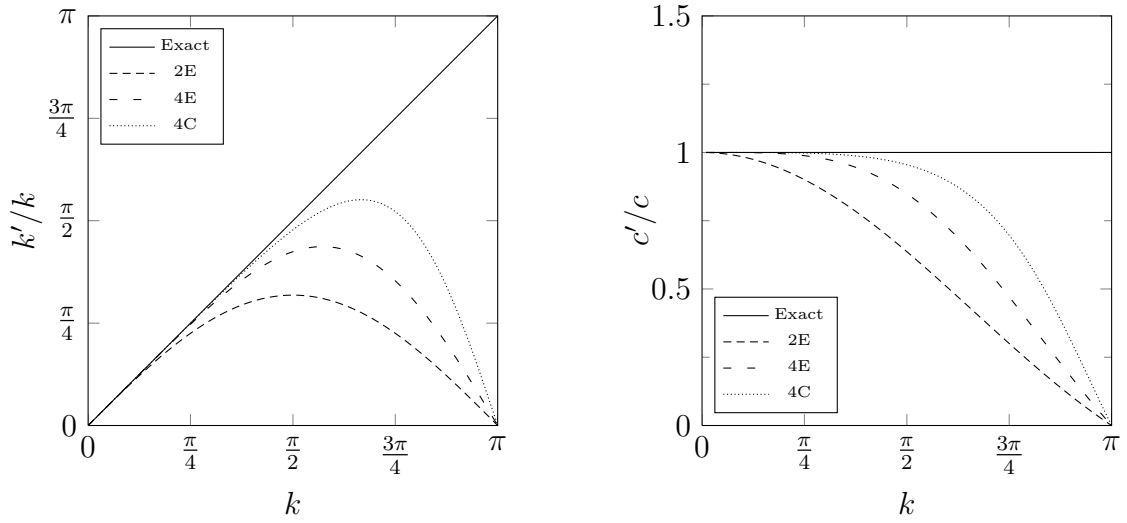

modifies the amplitude of the wave (*dissipation*), while the real part modifies the speed of the wave (*dispersion*). For centered operators, the modified wavenumber has no imaginary part and thus no built-in dissipation. The results of such analysis for the schemes of Table 1 are shown in Figure 1. On equal order of accuracy, the 4C scheme shows a better behaviour with respect to the explicit counterpart 4E. The better resolution of compact schemes is attributed to their *global* nature resembling spectral schemes, which makes them suitable for multi-scale flows.

Finally, note that two approximations are involved in the aforementioned methodology. First, the cartesian-like approach retains the formal accuracy of the interpolation scheme only in case of orthogonal grids. This is not an issue since only cartesian grids are considered here; however, in the general case of distorted grids, a multidimensional stencil has to be considered. Second, due to non-linearity of convective fluxes, the calculation of a face-averaged flux on the basis of interpolated face-averaged conservative variables is formally only second-order accurate. A number of possible remedies are currently under evaluation, and have not been taken into consideration here.

3.2.2 Diffusive fluxes

Unlike convective fluxes, diffusive terms are linear and do not raise specific difficulties. In the overwhelming majority of Navier-Stokes methods, they are calculated by a second-order centered formula. However, in the present work, also a fourth-order explicit centered scheme has been taken into account. Since diffusive fluxes depend on face-averaged derivatives of velocity and temperature, the resulting scheme is similar to Eq. (8), with face-averaged derivatives appearing on the left-hand side. The two resulting schemes will be indicated in the following by $2\mathrm{E_d}$ and $4\mathrm{E_d}$.

3.3 Time advancement

Once the convective and diffusive fluxes have been discretized, Eq. (4) reduces to a system of ordinary differential equations:

$$V_{ijk}\frac{d\bar{\mathbf{U}}_{ijk}}{dt} = \mathbf{R}_{ijk}, \tag{9}$$

where $\mathbf{R}_{ijk}$ is the *residual* resulting from spatial discretization. Time integration is achieved by standard explicit Runge-Kutta schemes:

$$\bar{\mathbf{U}}^{n+1} = \bar{\mathbf{U}}^{n} + \Delta t \sum_{l=1}^{s} b_l \mathbf{R}^l \tag{10}$$

$$\mathbf{R}^l = \mathbf{R}\left(\bar{\mathbf{U}}^{n} + \Delta t \sum_{m=1}^{l-1} a_{lm}\mathbf{R}^m\right), \tag{11}$$

where s is the number of stages, b_l and a_{lm} are the Runge-Kutta coefficients and the subscript ijk has been omitted for clarity. Runge-Kutta methods are widely used in numerical simulations of both incompressible and compressible turbulence, due to their ease of implementation and relatively large stability footprint. Moreover, they have the advantage over multistep methods of being self-starting, i.e., information from previous time-levels is not required. For standard explicit schemes, the temporal order of accuracy is typically equal to the number of stages, at least for $s \leq 4$. The code handles explicit schemes with arbitrary stages; in this work, a third-order method is employed.

The stability characteristics resulting from the coupling between Runge-Kutta methods and the spatial schemes described in §3.2 can be again derived by analyzing a linear advection equation. The result is $\frac{c\Delta t}{\Delta x} \leq \frac{\sigma_i}{w'_m}$, where σ_i depends on the stability segment of the time-advancement method on the imaginary axis, while w'_m is the maximum value of k' achieved by the spatial operator in Figure 1 [6]. To give an example, third-order Runge-Kutta methods used in conjunction with the schemes 2E, 4E and 4C have an acoustic CFL limit of $\sqrt{3}$, 1.262 and 1, respectively. It can be concluded that the time-stepping restriction becomes more severe as the resolution of the method increases.

3.4 Stability and robustness

Stability and robustness are likely to be the most difficult goals to be combined with low-dissipation and high-order accuracy requirements. In fact, it is well-known that centered difference schemes can exhibit instabilities when used at small viscosities (i.e., high Reynolds numbers), due to accumulation of aliasing errors, imperfect boundary conditions or skewed grids. The lack of any built-in damping mechanism may allow the growth of high-frequency modes and lead to erroneous results or to a blow-up of the computation. An ideal discretization algorithm should be able to prevent, or suppress, any source of instability while keeping high accuracy and reasonable computational cost. A number of possible solutions are available in the code, namely second- and fourth-order artificial dissipation terms [12] and a compact low-pass filter [13]:

$$\alpha_f \hat{\mathbf{U}}_{i-1} + \hat{\mathbf{U}}_i + \alpha_f \hat{\mathbf{U}}_{i+1} = \sum_{l=-L_f}^{L_f} \hat{\gamma}_l \left(\bar{\mathbf{U}}_{i+l} \right), \tag{12}$$

where α_f controls the strength of the filter and ranges from $-1/2$ to $1/2$, and L_f determines the filter order. Finally, note that the 2E scheme, as obtained by Eqs. (7) and (8), is cast in a so-called *skew-symmetric-like* form. Although this method does not preserve kinetic energy exactly at a discrete level, it has proved to be more stable with respect to a standard conservative form [9]. Further refinements are currently under development.

4 RESULTS

4.1 Two-dimensional vortical flow

As a first numerical experiment, the convection of a subsonic two-dimensional vortex in a periodic box is investigated. The aim of the test is to check the capability of the numerical schemes to accurately convect vortical structures over long times, and was also proposed by CERFACS as a benchmark to compare the accuracy of several DNS/LES codes [10]. The initial condition is given by the streamfunction:

$$\Psi(x, y) = \Gamma \exp\left(-\frac{x^2 + y^2}{2R^2} \right), \tag{13}$$

where Γ and R are related to the strength and the size of the vortex, respectively. The associated velocity field is calculated by the relations $u = U_\infty + \frac{\partial \Psi}{\partial y}$ and $v = -\frac{\partial \Psi}{\partial x}$, whereas the pressure field is given by

$$p(x, y) = p_0 - \frac{\rho_0 \Gamma^2}{2R^2} e^{-\frac{x^2+y^2}{R^2}}. \tag{14}$$

The temperature field is uniform ($T = 300\text{K}$), while density is calculated by the equation of state, with $p_0 = 1\text{atm}$. The vortex is convected at a Mach number $M = 0.1$ within a

Figure 2: y-component of the velocity along the centerline after 10 (*left*) and 40 (*right*) turnover times

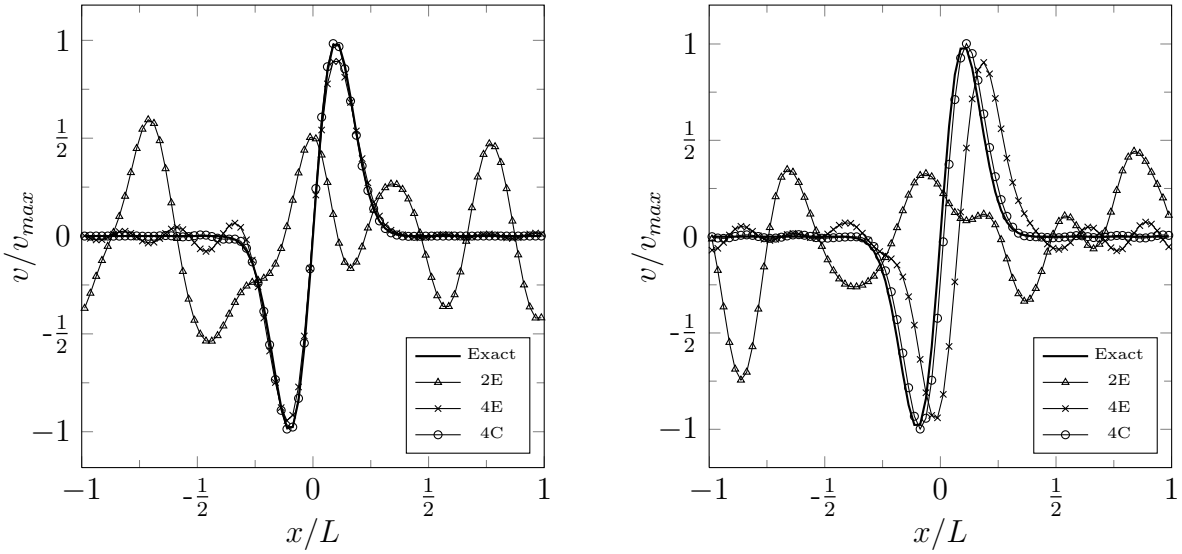

square periodic box of length L, with $R = L/20$ and $\Gamma = v_{max}R\sqrt{e}$, where $v_{max} = U_\infty/25$. The domain is discretized by a uniform mesh with spacing $\Delta/R = 0.25$.

The vortex is expected to travel without deformation. In Figure 2, results are shown for the three schemes listed in Table 1; all tests have been performed with a third-order Runge-Kutta scheme with an acoustic CFL of 0.7. The fourth-order methods perform remarkably well, especially the compact one, which preserves the vortical structure with minimum phase-lag after 40 turn-over times; on the contrary, the explicit scheme presents small oscillations due to its dispersive character. The 2E scheme is completely distorted already after 10 turn-over times, revealing its inadequacy for high-fidelity simulations. The simulations have required, on average, about $2\mu s$/it/cell on an Intel Xeon 2.7 GHz processor. The performances are excellent in comparison with other similar codes [10].

4.2 Taylor-Green vortex

The three-dimensional Taylor-Green vortex is an excellent test-case for LES and DNS codes, as it comprises the key processes of turbulence in a very simple configuration. A triperiodic cube is filled by the initial conditions:

$$u(x, y, z) = U_0 \sin(x) \cos(y) \cos(z) \tag{15a}$$

$$v(x, y, z) = -U_0 \cos(x) \sin(y) \cos(z) \tag{15b}$$

$$p(x, y, z) = p_0 + \frac{\rho_0 U_0^2}{16} \left[\cos(2x) + \cos(2y)\right] \left[\cos(2z) + 2\right]. \tag{15c}$$

As time advances, the initial distribution of vorticity is subject to vortex-stretching, thus generating small scales and eventually causing the vortices to break into turbulence. Since

there is no forcing to sustain the turbulent motion, a decay is observed after transition. The problem was also one of the tests proposed for the First International Workshop on High-Order Methods in CFD, held in Nashville in 2012.

The incompressible problem is entirely governed by the Reynolds number, equal to 1600. However, since the code solves the compressible flow equations, the other dimensional parameters have been set to yield a nearly incompressible condition, i.e. $M = 0.1$. The domain consists of a periodic cube with sides of 2π, which has been discretized by a uniform mesh of increasing resolution, 64^3, 128^3 and 256^3 cells.

The usual diagnostic parameters for assessing a numerical solution of the problem are the time-evolution of the global kinetic energy dissipation rate

$$\varepsilon = \frac{d}{dt}\frac{1}{\rho_0 \Omega}\int_\Omega \rho \frac{u_i u_i}{2} d\Omega, \tag{16}$$

and of the integrated enstrophy

$$\zeta = \frac{1}{\rho_0 \Omega}\int_\Omega \rho \frac{\omega_i \omega_i}{2} d\Omega. \tag{17}$$

The latter is an indirect measure of the dissipation rate, through the relation $\varepsilon_\zeta = 2\frac{\mu}{\rho_0}\zeta$.

Figure 3: Dissipation rate as a function of the non-dimensional time t^* for different resolutions, schemes and filters

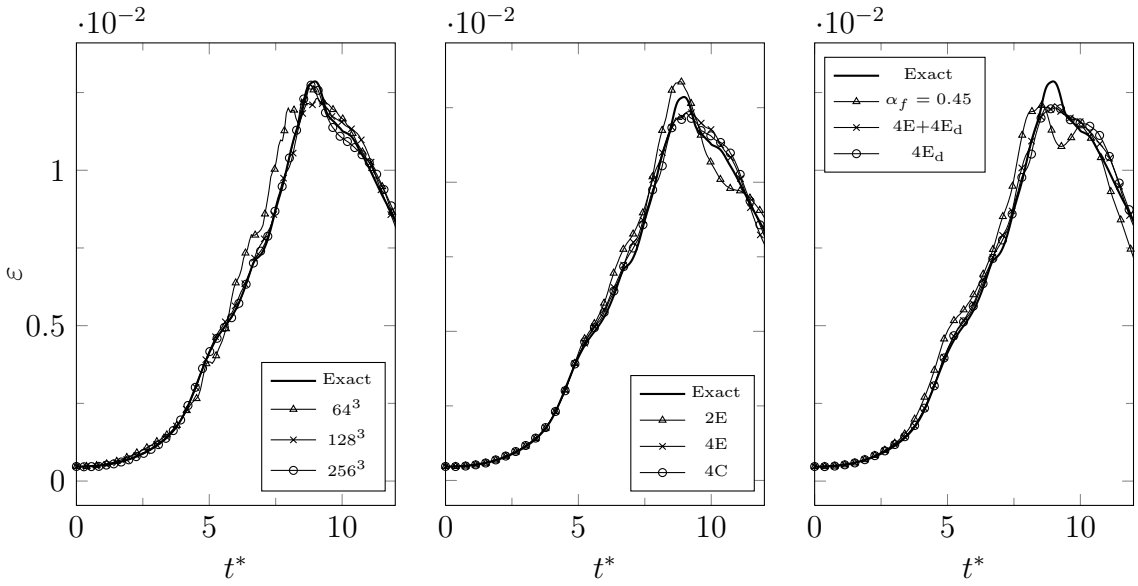

The computed time-evolution of ε and ε_ζ is shown in Figures 3 and 4, respectively, for different resolutions, schemes and filters. A reference solution obtained by a pseudo-spectral code is also reported for comparison [11]. Where not otherwise specified, results

Figure 4: Enstrophy-based dissipation rate as a function of the non-dimensional time t^* for different resolutions, schemes and filters

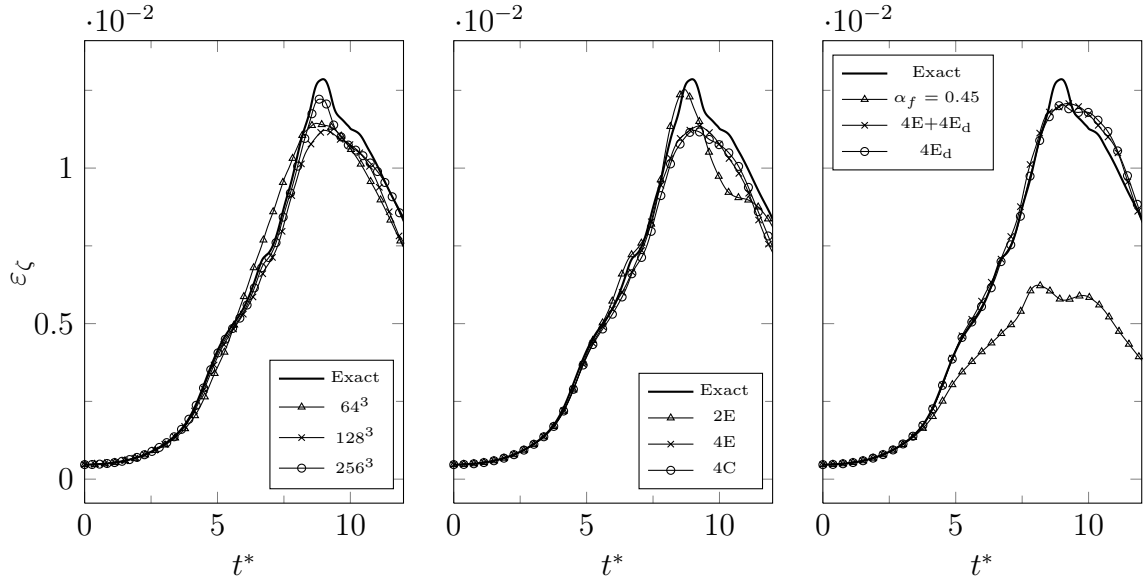

are obtained on the 128^3 grid, using the scheme 4C for convective fluxes, $2\mathrm{E_d}$ for diffusive fluxes and without filter. On a discrete level, the two quantities ε and ε_ζ have a different meaning: the former comprises all sources of dissipation (physical as well as numerical), while the latter is solely due to vorticity and hence does not take into account any form of artificial dissipation. The fourth-order schemes are in very good agreement with the reference solution, both on the 128^3 and the 256^3 grids and for both the energy- and enstrophy-based dissipation rates. This means that no spurious dissipation is added to the solution and turbulent scales are well resolved by the numerical scheme at any resolution. As expected, the scheme adopted for the diffusive fluxes does not seem to have a significant influence. The effect of the filter is mainly revealed by the enstrophy-based dissipation rate: by removing a part of the energy-dissipating turbulent structures, the resulting dissipation-rate is lessened accordingly.

5 CONCLUSIONS

The main elements of the computational core of the CIRA code SPARK-LES have been described. Numerical experiments show that the code is highly efficient and very accurate for basic, but representative, benchmarks. The best available scheme (fourth-order compact) performs remarkably well for both convection of a subsonic vortex and the challenging Taylor-Green vortex problem. Further numerical and physical models are being implemented and validated in the code in order to be able to simulate more complex test cases including real gas effects and combustion in low and high pressure conditions.

REFERENCES

[1] Candel, S., Durox, D., Schuller, T., Darabiha, N., Hakim, L. and Schmitt, T. Advances in combustion and propulsion applications. *Eur. J. Mech. B-Fluid* (2013) **40**:87–106.

[2] Pitsch, H. Large-eddy simulation of turbulent combustion. *Annu. Rev. Fluid Mech.* (2006) **38**:453–482.

[3] Schmitt, T., Méry, Y., Boileau, M. and Candel, S. Large-eddy simulation of oxygen/methane flames under transcritical conditions. *Proc. Combust. Inst.* (2011) **33**:1383–1390.

[4] Borrelli, S., et al. The HYPROB Program: mastering key technologies, design and testing capabilities for space transportation rocket propulsion evolution. *63th International Astronautical Congress*, Naples, (2012).

[5] Ferziger, J.H. and Peric, M. *Computational methods for fluid dynamics*. Springer, 3rd Edition, (2002).

[6] Lele, S.K. Compact finite difference schemes with spectral-like resolution. *J. Comput. Phys.* (1992) **103**:16–42.

[7] Lacor, C., Smirnov, S. and Baelmans, M. A finite volume formulation of compact central schemes on arbitrary structured grids. *J. Comput. Phys.* (2004) **198**:535–566.

[8] Fosso P., A., Deniau, H., Sicot, F. and Sagaut, P. Curvilinear finite-volume schemes using high-order compact interpolation. *J. Comput. Phys.* (2010) **229**:5090–5122.

[9] Ducros, F., Laporte, F., Souleres, T., Guinot, V., Moinat, P. and Caruelle, B. High-order fluxes for conservative skew-symmetric-like schemes in structured meshes: application to compressible flows. *J. Comput. Phys.* (2000) **161**:114-139.

[10] http://elearning.cerfacs.fr/numerical/benchmarks/vortex2d/index.php

[11] van Rees, W.M., Leonard, A., Pullin, D.I. and Koumoutsakos, P. A comparison of vortex and pseudo-spectral methods for the simulation of periodic vortical flows at high Reynolds numbers. *J. Comput. Phys.* (2011) **230**:2794–2805.

[12] Jameson, A., Schmidt E. and Turkel, E. Numerical solution of the Euler equations by finite volume methods using Runge-Kutta time-stepping schemes. *AIAA 14th Fluid and Plasma Dynamic Conference*, Palo Alto, (1981).

[13] Visbal, M.R. and Gaitonde, D.V. On the use of higher-order finite-difference schemes on curvilinear and deforming meshes. *J. Comput. Phys.* (2002) **181**:155-185.